

SMART: Advancing Scalable Map Priors for Driving Topology Reasoning

Junjie Ye^{1*}, David Paz², Hengyuan Zhang^{3*}, Yuliang Guo², Xinyu Huang²,
Henrik I. Christensen³, Yue Wang¹, and Liu Ren²

Abstract—Topology reasoning is crucial for autonomous driving as it enables comprehensive understanding of connectivity and relationships between lanes and traffic elements. While recent approaches have shown success in perceiving driving topology using vehicle-mounted sensors, their scalability is hindered by the reliance on training data captured by consistent sensor configurations. We identify that the key factor in scalable lane perception and topology reasoning is the elimination of this sensor-dependent feature. To address this, we propose SMART, a scalable solution that leverages easily available standard-definition (SD) and satellite maps to learn a map prior model, supervised by large-scale geo-referenced high-definition (HD) maps independent of sensor settings. Attributed to scaled training, SMART alone achieves superior offline lane topology understanding using only SD and satellite inputs. Extensive experiments further demonstrate that SMART can be seamlessly integrated into any online topology reasoning methods, yielding significant improvements of up to 28% on the OpenLane-V2 benchmark. Project page: <https://jay-ye.github.io/smart>.

I. INTRODUCTION

In recent years, lane perception and topology reasoning of driving scenes has received considerable attention, providing essential information about the structure and connectivity of road elements for autonomous driving and driver assistance systems. While previous map perception methods [1]–[4] primarily focus on identifying road markers, *e.g.*, lane dividers, road boundaries, and pedestrian crossings, driving topology reasoning encompasses the broader understanding of not only the lane geometry but also their connectivity and relationships with traffic elements, such as traffic lights and road signs. Such in-depth topological reasoning is essential for downstream tasks such as trajectory prediction, path planning, and motion control [5]–[7].

In the literature, driving topology is formulated as a graph that captures the location of lane centerlines and traffic elements, along with the connectivity between centerlines and their relationships to each traffic element [8]. Recent advancements [9]–[11] have shown promising progress in this field. Nevertheless, existing approaches face significant limitations. They are trained on data captured with consistent sensor configurations. Scaling these models typically requires

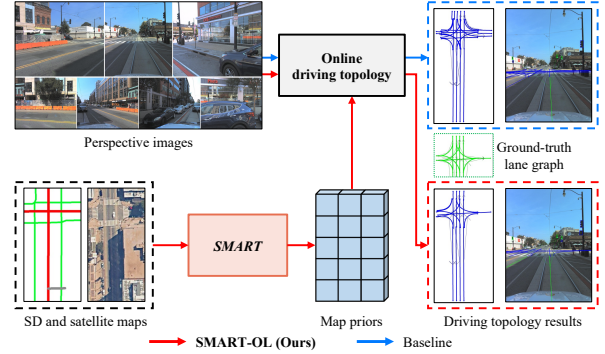


Fig. 1: Comparison between baseline and SMART-OL. Existing topology reasoning methods suffer from limited sensor data. SMART augments online topology reasoning with robust map priors learned from scalable SD and satellite maps, substantially improving lane perception and topology reasoning.

large datasets collected from vehicles with uniform sensor setups, which is both costly and time-consuming. Moreover, the low perspective of ground-based vehicles leads to occlusions from other vehicles, buildings, and objects, posing substantial challenges. Some recent works [8], [12], [13] aim to mitigate these occlusions by integrating standard definition (SD) maps with sensor inputs to provide geometric and topological priors. Yet, despite the widespread availability of SD maps, these approaches remain constrained by the limited availability of sensor data for training.

Training models for driving topology reasoning also requires access to high-definition (HD) maps associated with sensor data. Although these models are sensor-dependent, the supervision signals—HD maps—are calibrated to the real world and are geo-referenced. Setting aside the dependency on sensor data, there exists large-scale HD maps independently of sensor sets. For example, as shown in Table I, the motion forecasting set of Argoverse 2 [14] possesses HD maps from 285 times more scenes than those typically used for online mapping, not to mention HD maps available from many other sources [15], [16]. The extensive scale of HD maps offers a huge potential for learning generalizable map priors.

On the other hand, SD maps and satellite images are universally accessible from crowd sources [17], [18] with geo-locations. These *geospatial* maps offer powerful priors for understanding lane structures and are updated at a reasonable frequency. This leads us to an important question: *Can we advance scalable online topology reasoning with easily accessible geospatial maps and large-scale HD maps?*

We address this challenge by proposing a simple yet effective two-stage driving topology reasoning pipeline. As

*Work done while interned at Bosch Research North America.

¹Thomas Lord Department of Computer Science, University of Southern California {yejunjie, yue.w}@usc.edu

²Bosch North America and Bosch Center for AI (BCAI) {david.pazruiz, yuliang.guo2, xinyu.huang, liu.ren}@us.bosch.com

³Contextual Robotics Institute, UC San Diego {hyzhang, hichristensen}@ucsd.edu

TABLE I: Statistics of available HD maps in different datasets. The motion forecasting set from Argoverse (AV) 2 [14] has over 280 times more scenes compared to the sensor datasets.

Datasets	Num. of scenes	Num. of HD maps
AV 2 sensor - <i>train</i>	700	22,477
nuScenes - <i>train</i>	700	27,968
AV 2 motion forecasting - <i>val</i>	24,988	549,736
AV 2 motion forecasting - <i>train</i>	199,908	4,397,976

illustrated in Fig. 1, in the first stage, we introduce *SMART*, a map prior model targeted at reason lane topology using SD and satellite maps, supervised by large-scale HD maps. In the second stage, *SMART* is integrated with *online* topology reasoning models, enhancing them with powerful map priors learned from the first stage. This approach shifts the dependency on massive high-quality sensor data with consistent configurations to highly accessible and scalable geospatial maps, enabling scaled learning of adaptable map representations. The well-trained *SMART*, in turn, provides robust priors that significantly enhance the generalizability of online topology reasoning. Remarkably, our map prior model alone achieves state-of-the-art *offline* lane topology¹ given only SD and satellite inputs. Extensive experiments further demonstrate that integrating *SMART* into existing methods boosts performance by a large margin.

To summarize, our contributions are three-fold:

- A simple yet effective architecture for map prior learning at scale, achieving impressive lane topology reasoning with SD and satellite inputs.
- A map prior model that can be seamlessly integrated into any topology reasoning framework, enhancing robustness and generalizability.
- Evaluations on the widely-used benchmark [8] underscore the effectiveness of *SMART* in driving topology reasoning, achieving state-of-the-art performance.

II. RELATED WORKS

A. Online Mapping

Online mapping seeks to perceive lane structures on the fly, offering instant scene information for downstream tasks, in contrast to offline methods that rely on traffic observations [19] or aerial images [20], [21]. Early works primarily focus on estimating the geometry of road elements [1]–[4]. As one of the pioneering works, HDMapNet [1] generates an online semantic map, followed by post-processing to obtain vectorized road elements. Liu *et al.* [2] model vectorized HD map learning in an end-to-end fashion. Liao *et al.* [3], [4] propose a permutation invariant loss that boosts map geometry learning. Recent efforts have extended online mapping to include topology reasoning, which involves understanding the connectivity and relationships between lanes and traffic elements [8]–[10], [22]. Graph-based approaches like TopoNet [9] use scene graph neural networks to model these relationships, while simpler models like TopoMLP [10] still achieve promising improvements in topology reasoning

¹We refer to generating lane graphs from *offline* SD and satellite maps as *offline* lane topology.

with multilayer perceptrons (MLPs). Other methods [22], [23] explore novel ways to improve the initialization of 3D queries and interpret geometric distances for better topology reasoning. However, a common bottleneck for these methods is the reliance on large amounts of sensor data collected under consistent configurations.

B. Map Priors

Incorporating prior knowledge has been shown to advance online mapping performance [12], [13], [24]–[27]. Xiong *et al.* [24] assume a multi-traversal setting to enhance map perception with features from previous traversals. More recently, some works [12], [13] integrate SD maps with surroundings view images for joint training, demonstrating improved topology modeling performance. Similarly, Gao *et al.* [25] aid road element detection with satellite imagery. In spite of promising improvements achieved, priors introduced in these works remain consistently coupled to limited sensor data, leading to unsatisfying scalability. By contrast, we aim to learn a unified map prior representation from massive geospatial maps, featuring generalizability to novel locations and compatibility with any online topology reasoning models. Additionally, we identify the benefits of combining the road-level topology priors from SD maps and comprehensive bird’s eye view (BEV) textures from satellite maps.

III. METHODOLOGY

A. Problem Definition

Driving topology reasoning aims to perceive the geometric layout of lane centerlines \mathbf{V}_1 and traffic elements \mathbf{V}_t , and reason lane-to-lane connectivity \mathbf{E}_{1l} and lane to traffic element relationship \mathbf{E}_{lt} . They formulate two graphs, *i.e.*, $(\mathbf{V}_1, \mathbf{E}_{1l})$ and $(\mathbf{V}_t \cup \mathbf{V}_1, \mathbf{E}_{lt})$. Specifically, \mathbf{V}_1 consists of a set of directed lane instances with each denoted as $\mathbf{v}_1 = [p_0, \dots, p_{n-1}]$, where $p = (x, y, z) \in \mathbb{R}^3$.

Existing works estimate lane topology directly from perspective images captured by C synchronized surround-view cameras mounted to the ego-vehicle, some with SD maps as additional input. This line of work lacks scalability and generalizability due to its dependence on sensor data.

The pipeline of the proposed approach is shown in Fig. 2. During inference, we first fetch SD and satellite maps corresponding to the desired GPS location and adopt a well-trained map prior model to extract prior features. These features are then integrated into online topology reasoning models for enhanced centerline detection and relation modeling. To tackle the limited availability of sensory data and make full use of easily accessible SD and satellite maps, we decouple prior and sensor inputs with two-stage training.

B. Offline Map Prior Learning

In the first stage, we train a map prior model, referred to as *SMART*, with the goal of inferring lane graphs $(\mathbf{V}_1, \mathbf{E}_{1l})$ from offline SD and satellite maps.

Remark 1: We focus on lane graph modeling only in the first stage due to the invisibility of traffic elements like traffic lights and signs from the aerial perspective.

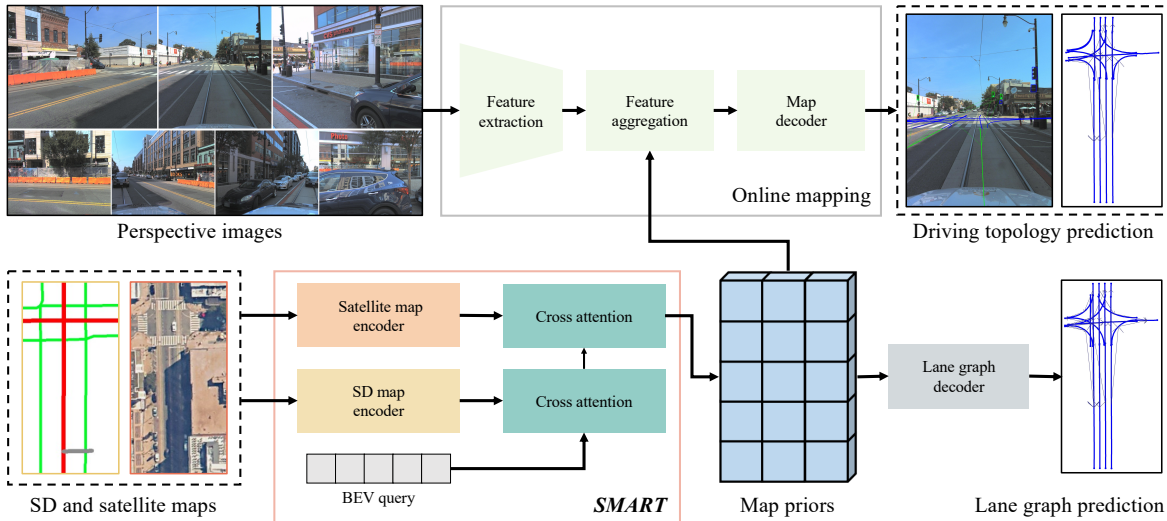


Fig. 2: Outline of the proposed approach. In the first stage (bottom row), SMART is trained at scale using SD and satellite maps for lane graph prediction, supervised by large-scale geo-referenced HD maps. In the second stage (top row), the robust map priors learned by SMART are seamlessly integrated into any online driving topology reasoning models, significantly enhancing lane perception and topology reasoning.

1) *SD map fetching*: We fetch SD maps from OpenStreetMap (OSM) [17] as in previous work [12], [13]. SD maps supply comprehensive geographic information for locations worldwide. Given a specific GPS location and orientation, we extract a local SD map that contains m road polylines $\mathbf{R} = [\mathbf{r}_1, \dots, \mathbf{r}_m]$. Each polyline is represented as an ordered set of 2D points and includes k associated attributes $\alpha \in \mathbb{R}^{m \times k}$ such as road types and lane counts. The number of polylines and their individual lengths may vary. The extracted map is then rotated and cropped to generate an ego-centric view covering the desired spatial range.

2) *Satellite map fetching*: We obtain satellite maps from the Mapbox Raster Tiles API [18], which segments the Earth’s surface into a grid of tiles at various zoom levels. By projecting a given GPS coordinate onto the 2D map tile plane, we identify the appropriate tile indices and query the API to retrieve the relevant tiles. The zoom level is set to 20, corresponding to ~ 0.11 meters per pixel. Through a process of map tile stitching, rotation, and cropping, we generate the satellite map $\mathbf{S} \in \mathbb{R}^{H \times W}$ that aligns with a specific location, orientation, and spatial range.

3) *SD and satellite map encoding*: For SD maps, we begin by evenly sampling N points along each polyline, then pad the number of polylines to m' to maintain a consistent count across maps within each training batch. This reformulates each SD map as $\mathbf{R}' = [\mathbf{r}'_1, \dots, \mathbf{r}'_{m'}, \mathbf{0}, \dots]_{m'}$ and $\alpha' \in \mathbb{R}^{m' \times k}$, where $\mathbf{r}' \in \mathbb{R}^{N \times 2}$. Following [12], we transform \mathbf{R}' from 2D coordinates to corresponding sinusoidal embeddings $\mathbf{R}'' \in \mathbb{R}^{m' \times Nd}$ with d dimensions using sinusoidal encodings E_{sin} :

$$\mathbf{R}'' = E_{\text{sin}}(\mathbf{R}') \quad . \quad (1)$$

With the refined road polylines \mathbf{R}'' and associated attributes α' , we generate SD map features $\mathbf{F}_{\text{SD}} \in \mathbb{R}^{m' \times C}$ with a linear layer and a Transformer [28] encoder:

$$\mathbf{F}_{\text{SD}} = \text{Enc}(\text{Linear}(\text{Concat}(\mathbf{R}'', \alpha')), \mathbf{M}) \quad , \quad (2)$$

where \mathbf{M} is a binary mask indicating valid polylines.

For satellite maps, we adopt an image backbone \mathcal{F} to extract features as $\mathbf{F}_{\text{Sate}} = \mathcal{F}(\mathbf{S})$ and flatten them to the dimension of $\mathbf{F}_{\text{Sate}} \in \mathbb{R}^{H_f W_f \times C}$.

To encode SD and satellite maps as a unified prior feature, we sequentially cross-attend features extracted from SD and satellite maps to a BEV feature map encoded with position embeddings, denoted as $\mathbf{B} \in \mathbb{R}^{H_B W_B \times C}$. Therefore, the fused prior features $\mathbf{B}_{\text{prior}}$ can be obtained as:

$$\begin{aligned} \hat{\mathbf{B}} &= \text{Softmax}(\mathbf{B} \mathbf{F}_{\text{SD}}^{\top}) \mathbf{F}_{\text{SD}} \\ \mathbf{B}_{\text{prior}} &= \text{Softmax}(\hat{\mathbf{B}} \mathbf{F}_{\text{Sate}}^{\top}) \mathbf{F}_{\text{Sate}} \end{aligned} \quad . \quad (3)$$

4) *Offline lane graph decoding*: To decode the lane graph from the prior features $\mathbf{B}_{\text{prior}}$, we begin by attending them to learnable centerline instance queries $\mathbf{Q} \in \mathbb{R}^{N_L \times C}$ with decoder layers in deformable DETR [29] that combine self-attention, deformable attention, and feed-forward network. Sequentially, we adopt the simplified GCN in [9] to modulate \mathbf{Q} for enhanced relational modeling. Hence, the enhanced instance queries $\hat{\mathbf{Q}}$ is formulated as:

$$\hat{\mathbf{Q}} = \text{GCN}(\text{Dec}(\mathbf{Q}, \mathbf{B}_{\text{prior}})) \quad . \quad (4)$$

Next, two sets of three-layer MLPs are adopted to classify and regress N_L lanes, each with N_P points as follows:

$$\mathbf{c} = \text{MLP}_{\text{cls}}(\hat{\mathbf{Q}}) \quad \mathbf{P} = \text{MLP}_{\text{reg}}(\hat{\mathbf{Q}}) \quad , \quad (5)$$

where $\mathbf{c} \in \mathbb{R}^{N_L}$ are the confidence scores and $\mathbf{P} \in \mathbb{R}^{N_L \times (N_P \times 3)}$ are regressed lane sets.

On the other hand, to achieve topological reasoning, the instance query $\hat{\mathbf{Q}}$ is fed into 2 MLPs separately, resulting in $\hat{\mathbf{Q}}'_1$ and $\hat{\mathbf{Q}}'_2$, both with a shape of $N_L \times \frac{C}{2}$. These two features are then repeated along a new axis and concatenate together as $\Theta_{\text{ll}} \in \mathbb{R}^{N_L \times N_L \times C}$. Subsequently, a binary classifier is operated on Θ_{ll} to obtain the final topological matrix ϵ .

Consequently, the lane graph $(\mathbf{V}_1, \mathbf{E}_{\text{ll}})$ is predicted by further filtering out low-confidence centerlines in \mathbf{P} and ϵ .

5) *Learning objective*: Similar to existing works [9]–[11], the overall loss \mathcal{L} consisting of classification loss \mathcal{L}_{cls} , regression loss \mathcal{L}_{reg} , and topological loss \mathcal{L}_{top} is defined as:

$$\mathcal{L} = \mathcal{L}_{\text{cls}} + \mathcal{L}_{\text{reg}} + \mathcal{L}_{\text{top}} \quad , \quad (6)$$

where \mathcal{L}_{cls} and \mathcal{L}_{top} employ focal loss, \mathcal{L}_{reg} adopts L1 loss.

C. Online Topology Reasoning with SMART

The well-trained SMART can be seamlessly integrated into any online topology reasoning models, augmenting them with robust prior features derived from SD and satellite maps. Generally, there are two mainstream pipeline used in existing online approaches: BEV-based and perspective-based methods. The former [9], [11], [22] explicitly projects features extracted from surrounding views into the BEV perspective using BEVFormer [30], followed by perception and reasoning heads for topology prediction. In this pipeline, we directly substitute the learnable BEV queries with prior features extracted by SMART. Conversely, in perspective-based methods [10], [23], the lane decoder interacts directly with multi-view visual features for perception and topology reasoning. In this paradigm, we employ a cross-attention layer to align prior features with perspective features.

To mitigate the risk of overfitting due to the limited sensor data, the weights of SMART are kept fixed during the training of online topology models, which are trained with their original settings. We term online topology reasoning with SMART integrated as *SMART-OL*.

Remark 2: In practical applications, aside from fetching and inferring prior features online, these features can be precomputed using future geo-locations of the ego-vehicle derived from the navigation route or mission plans.

IV. EXPERIMENTS

In this section, we aim to answer the following questions: (1) How far can we get with SMART alone? (2) How much can SMART boost online topology reasoning? (3) How well can SMART generalize to unseen areas? (4) Can SMART benefit from scaled training data? (5) Can SD and satellite map fusion boost performance? (6) Can SMART reduce the reliance on sensor data?

A. Dataset and Metrics

1) *Dataset*: Without loss of generality, we utilize the Argoverse 2 motion forecasting dataset [14] for training SMART, which provides geo-referenced HD maps despite lacking associated sensor data. Ground-truth lane graphs are derived from these HD maps by regressing centerlines and connecting lanes based on topology [8]. Table I summarizes the number of scenes in different datasets, each comprising consecutive driving frames at 2 Hz, with each frame associated with an HD map segment. While traditional online mapping benchmarks like the Argoverse 2 sensor dataset [14] and nuScenes [31] provide only 700 driving scenes with fewer than 30k HD maps, the validation set of the motion forecasting dataset includes $\sim 25\text{k}$ scenes with over 549k HD maps. The training set contains $\sim 200\text{k}$ scenes and over

4.3 million HD maps—**285** times more scenes and over **160** times more HD data compared to sensor sets. This substantial increase in data amount and diversity supports the learning of significantly more generalizable and scalable map priors.

The evaluation is conducted on the primary set of the OpenLane-V2 dataset [8], which extends Argoverse 2 sensor set [14] with ground truth for traffic element detection and topology relationship association. The associated 7-view images are only available during training of online mapping.

We extract the corresponding ego-centric SD maps from OSM [17] and satellite images from Mapbox Raster Tiles [18] using the methods described in Sections III-B.1 and III-B.2. All maps are centered on the ego-vehicle’s position and oriented in the direction of travel, covering an area of $100\text{m} \times 50\text{m}$ along the longitudinal and lateral directions, respectively.

2) *Metrics*: We report the OpenLane-V2 Score (OLS) defined in [8], which is computed as:

$$\text{OLS} = \frac{1}{4} \left[\text{DET}_1 + \text{DET}_t + \sqrt{\text{TOP}_{11}} + \sqrt{\text{TOP}_{1t}} \right] \quad , \quad (7)$$

where DET_1 is the discrete Fréchet distance [33] mean average precision (mAP) for lane geometry, DET_t is the mAP for traffic elements. TOP_{11} and TOP_{1t} are the topology scores for lane-to-lane connectivity and lane-to-traffic-element relationship, respectively.

B. Implementation details

We implement SMART with PyTorch. The number of sampling points N in SD maps is set to 11. We adopt a 6-layer Transformer encoder as the SD map encoder. For satellite map encoding, we first resize satellite images to 500×250 and then utilize ResNet-50 [34] pretrained on ImageNet [35] as the backbone for features extraction. Multi-scale features from the last three stages of ResNet-50 are employed and cross-attended with a BEV feature map \mathbf{B} , which has a size of $H_B = 200$, $W_B = 100$, and $C = 256$. The number of centerline queries N_L is set to 200. To keep the training time manageable while maintaining the diversity of HD maps, we sample frames in each scene with a frame rate of 0.5 and filter out still frames. This results in 200k scenes with 810k HD maps, which are used to train SMART in the first stage, unless otherwise specified. SMART is trained for 8 epochs with AdamW [36] optimizer on 8 NVIDIA A100 GPUs, which takes ~ 2 days to complete training. The batch size for each GPU is 12.

We integrate well-trained SMART into two state-of-the-art open-sourced baselines for second-stage training, namely

TABLE II: Comparison of SMART and online mapping methods on lane graph generation. Per-frame latency is measured by running individual methods on an Nvidia GeForce RTX 3090 GPU. Benefiting from scaled training, SMART outperforms *online* mapping methods on both lane perception and topology reasoning with *offline* geospatial maps.

Input type	Methods	DET_1	TOP_{11}	Latency (ms)
Perspective images	TopoNet	28.6	10.9	172.6
	TopoMLP	28.5	21.7	328.2
SD and satellite maps	SMART (Ours)	37.9	31.9	44.3

TABLE III: Overall performance comparison on the OpenLane-V2 Dataset. Integrating map prior features into online mapping pipelines, SMART-OL consistently boosts different kinds of online mapping pipelines by a wide margin, yielding state-of-the-art online driving topology reasoning performance.

Input type	Venues	Methods	DET _l	TOP _{ll}	DET _t	TOP _{lt}	OLS
Perspective images	ICCV 2021	STSU [32]	12.7	2.9	43.0	19.8	29.3
	ICML 2023	VectorMapNet [2]	11.1	2.7	41.7	9.2	24.9
	ICLR 2023	MapTR [3]	17.7	5.9	43.5	15.1	31.0
	Arxiv 2023	TopoNet [9]	28.6	10.9	48.6	23.8	39.8
	Arxiv 2024	TopoLogic [22]	29.9	23.9	47.2	25.4	44.1
	Arxiv 2024	Topo2D [23]	29.1	22.3	50.6	26.2	44.5
	ICLR 2024	TopoMLP [10]	28.5	21.7	49.5	26.9	44.1
	ECCV 2024	RoadPainter [11]	30.7	22.8	47.7	27.2	44.6
Perspective images + SD maps	IROS 2024	TopoOSMR [13]	30.6	17.1	44.6	26.8	42.1
	ICRA 2024	SMERF [12]	33.4	15.4	48.6	25.4	42.9
	Arxiv 2024	TopoLogic [22]	34.4	28.9	48.3	28.7	47.5
	ECCV 2024	RoadPainter [11]	36.9	<u>29.6</u>	47.1	29.5	48.2
Perspective images + Map priors	Ours	SMART-OL (TopoNet)	<u>46.1</u>	27.5	48.3	33.1	<u>51.1</u>
			+61.2%	+152.3%	-0.6%	+39.1%	+28.4%
		SMART-OL (TopoMLP)	46.6	37.0	47.7	<u>33.0</u>	53.1
		+63.5%	+70.5%	-3.6%	+22.7%	+20.4%	

TopoNet [9] and TopoMLP [10], which represent the BEV-based and perspective-based models, respectively. We maintain their default setting of using ResNet-50 as the image backbone for multi-view images. All other settings remain unchanged, except for the integration of map prior features from SMART, as described in Sec. III-C.

C. How far can we get with SMART alone?

SMART is trained to generate lane graphs solely from geospatial maps in the first stage. Naturally, this raises the question of how accurate the lane graphs predicted from SD and satellite maps are. In Table II, we compare SMART with two state-of-the-art *online* driving topology reasoning methods [9], [10] on the validation set of [8]. Metrics related to traffic elements are excluded due to the impracticality of detecting them from an aerial view. The results show that SMART achieves superior performance, with DET_l of 37.9 compared to 28.6 and 28.5 for TopoNet and TopoMLP. In terms of TOP_{ll}, SMART scores 31.9, significantly higher than TopoNet’s 10.9 and TopoMLP’s 21.7. Additionally, SMART shows significantly lower per-frame latency of 44.3 ms, which is 3.9× and 7.4× faster than online mapping models. Despite differences in input modality and the amount of training data, the remarkable performance of SMART underscores the abundant prior information contained in geospatial maps and the vast potential for scaling driving topology reasoning from a geospatial map perspective.

D. How much can SMART boost online topology reasoning?

In light of our goal to achieve robust *online* driving topology reasoning, we expect SMART also to yield state-of-the-art performance in *online* settings. Therefore, we train two kinds of online topology reasoning baselines [9], [10] jointly with map priors extracted by well-trained SMART, in comparison to baselines along with state-of-the-art approaches. All models are trained for 24 epochs on the training set of [8]. As shown in Table III, SMART-OL consistently improves baselines by over 20% on OLS. Notably, SMART-OL improves lane detection performances of both baselines by over 60%, and boosts TopoNet’s lane topology ability by

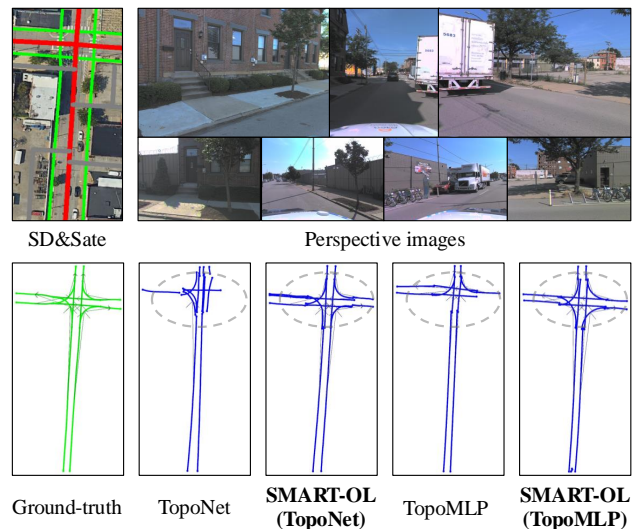


Fig. 3: Qualitative comparison of SMART-OL to baselines. The top-left shows the SD map plotted on top of the satellite image. Our method improves baselines consistently, producing more complete lane graphs.

152.3%. Owing to enhanced lane detection, the performance of lane-to-traffic-element topology is also improved by over 20%. In comparison to previous works which only introduce SD maps as priors, SMART-OL remains superior in all metrics. More specifically, TopoNet, when enhanced by SMART, substantially outperforms both SMERF [12] and TopoOSMR [13], which also use TopoNet as their baseline. Some qualitative comparisons are illustrated in Fig. 3, where SMART-OL generates more complete lane graphs compared to both baselines. These results verify the efficacy of adopting map priors from SMART to online mapping.

Remark 3: Since the traffic elements are detected directly from perspective images, as expected, the performance of SMART-OL on DET_t remains similar to the baselines.

E. How well can SMART generalize to unseen areas?

Previous works have identified that OpenLane-V2 [8] contains geographically overlapping areas between training and validation sets [12], [37]. To evaluate the performance of SMART compared to the baseline in completely unseen

TABLE IV: Evaluation in unseen areas. SMART-OL improves the baseline on all metrics, especially on DET_t and TOP_{1l} .

Methods	DET_t	TOP_{1l}	DET_t	TOP_{1t}	OLS
Baseline	16.6	4.7	32.9	13.3	26.9
SMART-OL	24.7	11.7	34.7	16.7	33.6
Improvements (%)	48.8	148.9	5.5	25.6	24.9

TABLE V: Scaling studies for data size. The performances of SMART in both *offline* and *online* settings improve progressively as the amount of training data grows.

Data amount	Offline		Online					OLS
	DET_t	TOP_{1l}	DET_t	TOP_{1l}	DET_t	TOP_{1t}		
Base	33.0	16.2	34.8	20.9	47.9	27.7	45.3	
18×	34.5	28.9	43.8	24.0	48.0	31.6	49.3	
40×	37.9	31.9	46.1	27.5	48.3	33.1	51.1	

areas, we resplit the training and validation sets in [8], along with the data used for the first-stage training, ensuring geo-disjoint training and evaluation. The performance comparison on the geo-disjoint splits is shown in Table IV. Notably, SMART-OL improves the baseline in terms of lane detection by **48.8%** and lane topology reasoning by **148.9%**, yielding the OLS of 33.6, significantly improving baseline’s generalizability to novel areas.

F. Can SMART benefit from scaled training data?

Scaling law has been found in Transformer-based models, and scaling the data size generally leads to improved performance. In Table V, we experiment SMART with different amounts of training data, where *Base* corresponds to the number of HD maps in the training set of sensor dataset [14]. With the increases in data size to 18× and 40× larger, the performance of SMART in offline settings increases progressively. We also observe significant improvements in lane topology reasoning as data size increases, growing from 16.2 to 28.9 and 31.9 when trained with 18× and 40× larger data size, respectively. Improved performance in offline settings is consistent in online settings when enhancing the online model with the corresponding SMART trained offline. This scaling property verifies SMART’s great potential for generalizable topology reasoning in complex scenarios.

G. Can SD and satellite map fusion boost performance?

We empirically ablate SD or satellite maps to study the importance of each modality. As shown in Table VI, the elimination of either modality leads to a degradation in both offline and online settings, with the removal of satellite maps causing a more significant decline in performance. This observation suggests that lane-level textures contained in satellite images are crucial for topology reasoning. The superior performance yielded by fusing both modalities indicates that the structural information from SD maps and the semantics from satellite images complement each other.

H. Can SMART reduce the reliance on sensor data?

SMART trained on massive SD and satellite maps exhibits strong performance of topology reasoning. To investigate whether scaling up SMART can compensate for limited

TABLE VI: Ablation study on SD and satellite maps. The removal of either modality leads to a degradation in performance, indicating the necessity of fusing both.

Prior type	Offline		Online				
	DET_t	TOP_{1l}	DET_t	TOP_{1l}	DET_t	TOP_{1t}	OLS
SD maps	24.7	12.4	34.2	16.5	48.9	27.8	44.1
Satellite maps	35.1	23.4	41.2	22.2	48.7	30.7	48.1
SD and satellite maps	37.9	31.9	46.1	27.5	48.3	33.1	51.1

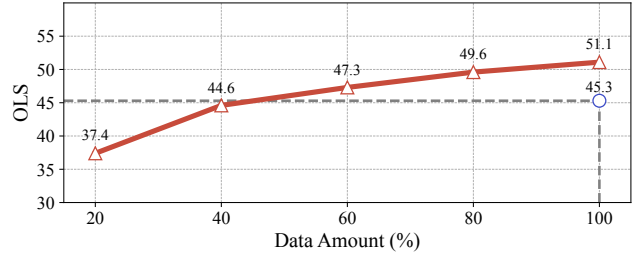


Fig. 4: Impact of varying sensor data availability. With only 40% of sensor data, SMART-OL achieves performance comparable to using the full sensor data, demonstrating its robustness with reduced sensor data.

sensor data in online mapping, we compare against the baseline online mapping model enhanced with SMART trained on geospatial maps corresponding to *sensor* set. We then progressively reduce the amount of sensor data used to train the online mapping model enhanced by SMART trained on *full* geospatial maps. As shown in Fig. 4, even with just 40% of sensor data, the model utilizing priors generated from *full* SMART achieves performance comparable to that of the model using priors from *sensor* SMART, which adopts the complete sensor dataset for training. This suggests that scaling up SMART can significantly enhance online mapping performance, even with reduced sensor data.

V. CONCLUSION AND FUTURE WORKS

This paper introduces SMART, offering a new perspective on scalable and generalizable driving topology reasoning while circumventing the need for extensive sensor data. By leveraging readily available geospatial maps and existing large-scale HD map datasets, SMART yields impressive offline topology reasoning and supplies robust map prior representations that can be seamlessly integrated into any online driving topology reasoning architectures, achieving state-of-the-art performance. More broadly, SMART opens up promising avenues for future research: (1) scaling up SMART in both model size and data to develop a comprehensive map foundation model, and (2) exploring the immense potential of map prior features for other tasks, such as trajectory prediction, motion planning, and end-to-end driving, wherever a robust understanding of lane structures is critical. We strongly believe that this work will considerably advance scalable and generalizable driving topology reasoning in autonomous driving.

ACKNOWLEDGMENT

We’d like to acknowledge our friends and colleagues, including Katie Z Luo, Cheng Zhao, Arun Das, Pranav Ganti, Nikhil Advani, and Sarthak Gupta, for their fruitful discussions and follow-ups.

REFERENCES

- [1] Q. Li, Y. Wang, Y. Wang, and H. Zhao, "HMapNet: An Online HD Map Construction and Evaluation Framework," in *Proceedings of the International Conference on Robotics and Automation (ICRA)*, 2022, pp. 4628–4634.
- [2] Y. Liu, T. Yuan, Y. Wang, Y. Wang, and H. Zhao, "VectorMapNet: End-to-end Vectorized HD Map Learning," in *Proceedings of the International Conference on Machine Learning (ICML)*, vol. 202, 2023, pp. 22 352–22 369.
- [3] B. Liao, S. Chen, X. Wang, T. Cheng, Q. Zhang, W. Liu, and C. Huang, "MapTR: Structured Modeling and Learning for Online Vectorized HD Map Construction," in *Proceedings of the International Conference on Learning Representations (ICLR)*, 2023, pp. 1–18.
- [4] B. Liao, S. Chen, Y. Zhang, B. Jiang, Q. Zhang, W. Liu, C. Huang, and X. Wang, "MapTRv2: An End-to-End Framework for Online Vectorized HD Map Construction," *International Journal of Computer Vision*, pp. 1–17, 2024.
- [5] A. Sadat, S. Casas, M. Ren, X. Wu, P. Dhawan, and R. Urtasun, "Perceive, Predict, and Plan: Safe Motion Planning Through Interpretable Semantic Representations," in *Proceedings of the European Conference on Computer Vision (ECCV)*, 2020, pp. 414–430.
- [6] N. Nayakanti, R. Al-Rfou, A. Zhou, K. Goel, K. S. Refaat, and B. Sapp, "Wayformer: Motion Forecasting via Simple & Efficient Attention Networks," in *Proceedings of the IEEE International Conference on Robotics and Automation (ICRA)*, 2023, pp. 2980–2987.
- [7] J. Mao, J. Ye, Y. Qian, M. Pavone, and Y. Wang, "A Language Agent for Autonomous Driving," in *Proceedings of the Conference on Language Modeling (COLM)*, 2024, pp. 1–40.
- [8] H. Wang, T. Li, Y. Li, L. Chen, C. Sima, Z. Liu, B. Wang, P. Jia, Y. Wang, S. Jiang, F. Wen, H. Xu, P. Luo, J. Yan, W. Zhang, and H. Li, "OpenLane-V2: A Topology Reasoning Benchmark for Unified 3D HD Mapping," in *Proceedings of the Advances in Neural Information Processing Systems (NeurIPS)*, vol. 36, 2023, pp. 18 873–18 884.
- [9] T. Li, L. Chen, H. Wang, Y. Li, J. Yang, X. Geng, S. Jiang, Y. Wang, H. Xu, C. Xu, J. Yan, P. Luo, and H. Li, "Graph-based Topology Reasoning for Driving Scenes," *arXiv preprint arXiv:2304.05277*, pp. 1–12, 2023.
- [10] D. Wu, J. Chang, F. Jia, Y. Liu, T. Wang, and J. Shen, "TopoMLP: A Simple yet Strong Pipeline for Driving Topology Reasoning," in *Proceedings of the International Conference on Learning Representations (ICLR)*, 2024, pp. 1–12.
- [11] Z. Ma, S. Liang, Y. Wen, W. Lu, and G. Wan, "RoadPainter: Points Are Ideal Navigators for Topology transformER," in *Proceedings of the European Conference on Computer Vision (ECCV)*, 2024, pp. 1–17.
- [12] K. Z. Luo, X. Weng, Y. Wang, S. Wu, J. Li, K. Q. Weinberger, Y. Wang, and M. Pavone, "Augmenting Lane Perception and Topology Understanding with Standard Definition Navigation Maps," in *Proceedings of the IEEE International Conference on Robotics and Automation (ICRA)*, 2024, pp. 4029–4035.
- [13] H. Zhang, D. Paz, Y. Guo, A. Das, X. Huang, K. Haug, H. I. Christensen, and L. Ren, "Enhancing Online Road Network Perception and Reasoning with Standard Definition Maps," in *Proceedings of the IEEE/RSJ International Conference on Intelligent Robots and Systems (IROS)*, 2024, pp. 1–9.
- [14] B. Wilson, W. Qi, T. Agarwal, J. Lambert, J. Singh, S. Khandelwal, B. Pan, R. Kumar, A. Hartnett, J. Kaesemodel Pontes, D. Ramanan, P. Carr, and J. Hays, "Argoverse 2: Next Generation Datasets for Self-Driving Perception and Forecasting," in *Proceedings of the Neural Information Processing Systems (NeurIPS) Track on Datasets and Benchmarks*, vol. 1, 2021, pp. 1–13.
- [15] H. Caesar, J. Kabzan, K. S. Tan, W. K. Fong, E. Wolff, A. Lang, L. Fletcher, O. Beijbom, and S. Omari, "NuPlan: A closed-loop ML-based planning benchmark for autonomous vehicles," *arXiv preprint arXiv:2106.11810*, pp. 1–5, 2021.
- [16] P. Sun, H. Kretschmar, X. Dotiwalla, A. Chouard, V. Patnaik, P. Tsui, J. Guo, Y. Zhou, Y. Chai, B. Caine, V. Vasudevan, W. Han, J. Ngiam, H. Zhao, A. Timofeev, S. Ettinger, M. Krivokon, A. Gao, A. Joshi, Y. Zhang, J. Shlens, Z. Chen, and D. Anguelov, "Scalability in Perception for Autonomous Driving: Waymo Open Dataset," in *Proceedings of the IEEE/CVF Conference on Computer Vision and Pattern Recognition (CVPR)*, 2020, pp. 2443–2451.
- [17] "Openstreetmap," <https://www.openstreetmap.org>, 2024, accessed: 2024-09-13.
- [18] "Mapbox Raster Tiles API," <https://docs.mapbox.com/api/maps/raster-tiles/>, 2025, accessed: 2025-01-29.
- [19] J. Zürn, I. Posner, and W. Burgard, "AutoGraph: Predicting Lane Graphs From Traffic Observations," *IEEE Robotics and Automation Letters*, vol. 9, no. 1, pp. 73–80, 2024.
- [20] M. Büchner, J. Zürn, I.-G. Todoran, A. Valada, and W. Burgard, "Learning and Aggregating Lane Graphs for Urban Automated Driving," in *Proceedings of the IEEE/CVF Conference on Computer Vision and Pattern Recognition (CVPR)*, 2023, pp. 13 415–13 424.
- [21] H. Blayney, H. Tian, H. Scott, N. Goldbeck, C. Stetson, and P. Angeloudis, "Bezier Everywhere All at Once: Learning Drivable Lanes as Bezier Graphs," in *Proceedings of the IEEE/CVF Conference on Computer Vision and Pattern Recognition (CVPR)*, 2024, pp. 15 365–15 374.
- [22] Y. Fu, W. Liao, X. Liu, H. xu, Y. Ma, F. Dai, and Y. Zhang, "TopoLogic: An Interpretable Pipeline for Lane Topology Reasoning on Driving Scenes," *arXiv preprint arXiv:2405.14747*, pp. 1–12, 2024.
- [23] H. Li, Z. Huang, Z. Wang, W. Rong, N. Wang, and S. Liu, "Enhancing 3D Lane Detection and Topology Reasoning with 2D Lane Priors," *arXiv preprint arXiv:2406.03105*, pp. 1–20, 2024.
- [24] X. Xiong, Y. Liu, T. Yuan, Y. Wang, Y. Wang, and H. Zhao, "Neural Map Prior for Autonomous Driving," in *Proceedings of the IEEE/CVF Conference on Computer Vision and Pattern Recognition (CVPR)*, 2023, pp. 17 535–17 544.
- [25] W. Gao, J. Fu, Y. Shen, H. Jing, S. Chen, and N. Zheng, "Complementing Onboard Sensors with Satellite Maps: A New Perspective for HD Map Construction," in *Proceedings of the IEEE International Conference on Robotics and Automation (ICRA)*, 2024, pp. 11 103–11 109.
- [26] Z. Jiang, Z. Zhu, P. Li, H.-a. Gao, T. Yuan, Y. Shi, H. Zhao, and H. Zhao, "P-MapNet: Far-Seeing Map Generator Enhanced by Both SDMap and HDMAP Priors," *IEEE Robotics and Automation Letters*, vol. 9, no. 10, pp. 8539–8546, 2024.
- [27] T. Yuan, Y. Mao, J. Yang, Y. Liu, Y. Wang, and H. Zhao, "PreSight: Enhancing Autonomous Vehicle Perception with City-Scale NeRF Priors," in *Proceedings of the European Conference on Computer Vision (ECCV)*, 2024, pp. 323–339.
- [28] A. Vaswani, N. Shazeer, N. Parmar, J. Uszkoreit, L. Jones, A. N. Gomez, L. u. Kaiser, and I. Polosukhin, "Attention Is All you Need," in *Proceedings of the Advances in Neural Information Processing Systems (NeurIPS)*, vol. 30. Curran Associates, Inc., 2017, pp. 1–11.
- [29] X. Zhu, W. Su, L. Lu, B. Li, X. Wang, and J. Dai, "Deformable DETR: Deformable Transformers for End-to-End Object Detection," in *Proceedings of the International Conference on Learning Representations (ICLR)*, 2021, pp. 1–16.
- [30] Z. Li, W. Wang, H. Li, E. Xie, C. Sima, T. Lu, Y. Qiao, and J. Dai, "BEVFormer: Learning Bird's-Eye-View Representation from Multi-Camera Images via Spatiotemporal Transformers," in *Proceedings of the European Conference on Computer Vision (ECCV)*, 2022, pp. 1–18.
- [31] H. Caesar, V. Bankiti, A. H. Lang, S. Vora, V. E. Liong, Q. Xu, A. Krishnan, Y. Pan, G. Baldan, and O. Beijbom, "nuScenes: A Multimodal Dataset for Autonomous Driving," in *Proceedings of the IEEE/CVF Conference on Computer Vision and Pattern Recognition (CVPR)*, 2020, pp. 11 618–11 628.
- [32] Y. B. Can, A. Liniger, D. P. Paudel, and L. Van Gool, "Structured Bird's-Eye-View Traffic Scene Understanding from Onboard Images," in *Proceedings of the IEEE/CVF International Conference on Computer Vision (ICCV)*, 2021, pp. 15 641–15 650.
- [33] T. Eiter and H. Mannila, "Computing discrete Fréchet distance," 1994.
- [34] K. He, X. Zhang, S. Ren, and J. Sun, "Deep Residual Learning for Image Recognition," in *Proceedings of the IEEE Conference on Computer Vision and Pattern Recognition (CVPR)*, 2016, pp. 770–778.
- [35] A. Krizhevsky, I. Sutskever, and G. E. Hinton, "ImageNet Classification with Deep Convolutional Neural Networks," in *Proceedings of the Advances in Neural Information Processing Systems (NeurIPS)*, F. Pereira, C. Burges, L. Bottou, and K. Weinberger, Eds., vol. 25, 2012, pp. 1–9.
- [36] I. Loshchilov and F. Hutter, "Decoupled Weight Decay Regularization," in *Proceedings of the International Conference on Learning Representations (ICLR)*, 2019, pp. 1–19.
- [37] A. Lilja, J. Fu, E. Stenborg, and L. Hammarstrand, "Localization Is All You Evaluate: Data Leakage in Online Mapping Datasets and How to Fix It," in *Proceedings of the IEEE/CVF Conference on Computer Vision and Pattern Recognition (CVPR)*, 2024, pp. 22 150–22 159.